

Article

Polyoxometalate Template-Based Synthetic Strategy to Prepare Ni, Mo Co-Doped CdS for Efficient Photocatalytic Hydrogen Evolution from Water Splitting

Jiawei Yan ^{1,2}, Zhidong Wei ^{1,2}, Meiqi Xu ^{1,2}, Zhi Jiang ^{1,2} and Wenfeng Shangguan ^{1,2,*}

¹ Research Center for Combustion and Environment Technology, Shanghai Jiao Tong University, Shanghai 200240, China; yanjerax@sjtu.edu.cn (J.Y.); weizhidong1013@126.com (Z.W.); xumeiqi@sjtu.edu.cn (M.X.); zhijiang@sjtu.edu.cn (Z.J.)

² Center of Hydrogen Science, Shanghai Jiao Tong University, NO. 800, Dongchuan Road, Shanghai 200240, China

* Correspondence: shangguan@sjtu.edu.cn; Tel.: +86-021-3420-6020

Received: 2 December 2020; Accepted: 15 December 2020; Published: 17 December 2020



Abstract: In this work, a novel polyoxometalate template-based strategy was applied to construct the bi-metal-doped CdS photocatalysts. NiMo₆ polyoxometalate template precursor was applied for the preparation of Ni, Mo co-doped CdS photocatalysts (NiMo-CdS). The structures of the materials were explored by XRD, SEM, HRTEM, HAADF, element mapping, XPS, Raman spectrum and UV-vis DRS. Moreover, the results of the UV-vis spectrum showed that NiMo-CdS exhibited an enhanced performance on light absorption. The results of photocatalytic hydrogen evolution from water splitting demonstrated that the NiMo-CdS showed higher efficiency on hydrogen evolution than noble-metal Pt-doped CdS. The reason could be ascribed to the enhanced light absorption ability and charge separation after Ni and Mo were introduced, which could also act as co-catalysts. The apparent quantum yield (AQY) efficiency could reach 42% at 365 nm. This work proposed a novel and inexpensive method to synthesize the bi-metal (Ni, Mo) decorated CdS photocatalysts for efficient hydrogen evolution from water splitting.

Keywords: photocatalytic; hydrogen; CdS; MoS₂; water splitting

1. Introduction

Photocatalytic water splitting has been proposed since Honda and Fujishima first reported it in 1972 [1]. Afterward, it ignited a majority of interests in photocatalytic water splitting for hydrogen production. Past decades have witnessed the development of photocatalysis on the materials and the intrinsic mechanisms [2–5]. Among them, TiO₂ was regarded as one of the most traditional materials [6–8]. However, the limitations constrained its application since it could only absorb the UV-light that occupied only 4% of the full arc solar spectrum. Furthermore, the low carrier mobility also makes efficiency lower than 1%. Therefore, it was urgent to explore the novel materials which could absorb the irradiation light from a wide range, like visible light, or even infrared light.

CdS, which could absorb visible light, has suitable energy band structures for photocatalytic hydrogen production from water splitting. In recent years, several works have reported CdS-based materials for hydrogen evolution [9–12]. The strategies could be mainly summarized as morphology design, solid solution method as well as heterojunction construction. Consequently, a majority of composites, like CdS/Co₉S₈ [13], ZnS/CdS [14], MnS/CdS [15], g-C₃N₄/CdS [16] and BiVO₄/CdS [17],

have been synthesized successfully and applied for photocatalytic hydrogen production, which was enhanced evidently after utilizing the mentioned strategies.

For promoting the photocatalytic activity, another critical factor was the co-catalysts in CdS-based photocatalysts, which also played an essential role in the procedure of photogenerated carrier transfer. MoS₂, which mainly has two different phases of 1T and 2H [18], was considered as the efficient co-catalyst in CdS-based materials [9,11]. Although large works have devoted much effort to the MoS₂-CdS-based materials, some researchers proposed that 1T MoS₂-CdS has a superior performance than 2H MoS₂-CdS. Therefore, obtaining a higher concentration of 1T-MoS₂ in MoS₂ co-catalysts was an urgent work and has ignited interest in the design of the photocatalysts [19–21].

Our previous study also investigated the properties of Ni-based co-catalysts with CdS as the photocatalysts, like Ni, NiO and Ni(OH)₂. The results showed that NiO species were tightly dispersed on the surface of CdS, which could enhance the photocatalytic performance [22–24]. Afterward, the 1T and 2H mixed phase of MoS₂ coupled with CdS as the photocatalyst also was synthesized [11]. The results exhibited an excellent activity on photocatalytic hydrogen evolution. However, suppose that the Ni-based co-catalysts and 1T-MoS₂ with a higher concentration could serve as the co-catalysts simultaneously, it will be favorable for the enhancement of the charge separation and light absorption and thus, improve the photocatalytic activity.

Recently, Huang et al. has presented a novel method to stabilize the 1T-MoS₂, which gained an ascendant performance in electrochemical hydrogen evolution [10]. In this work, the polyoxometalate was used as a template to synthesize the NiO/1T-MoS₂ composites. If this synthetic strategy could be applied in the construction of photocatalysts, the Ni, Mo co-doped CdS could be fulfilled via a simple method. However, relative works were rare. Consequently, in this work, NiO/1T-MoS₂ as a co-catalyst was prepared via the polyoxometalate template-based method in one-step. The results exhibited that the MoS₂ was mainly composed of the 1T phase and thus the photocatalytic ability was evidently improved. The AQY efficiency could reach 42% at under 365 nm. This work proposed a novel method for the construction of co-catalysts with non-noble metal in particulate photocatalytic water splitting, especially for the 1T-MoS₂ preparation strategy.

2. Results and Discussions

The powder X-ray diffraction (XRD) patterns of x%(NiMo₆)@CdS-τ (x = 5, 7.5, 10, τ = 12, 24, 36 h) composites are shown in Figure 1a–f, respectively. Although, after modification with variable amounts of NiMo₆ precursor and variable hydrothermal time, all XRD patterns turned out to be similar and all peaks of pristine CdS could be obviously detected in Figure 1a,c,e, according to Jade card No.01-0783. It implies that the introduction of Ni and Mo shows little influence on the bulk CdS structure. Despite this, Ni, Mo co-doping increases the lattice constant of the CdS structure, resulting in a small peak shift towards a lower angle, as shown in Figure 1b,d,f. Nonetheless, the crystalline structure of Ni and Mo species was still uncertain from the above XRD patterns, and hereafter, identified by X-ray photoelectron spectrum (XPS) measurements that will be discussed later.

The morphology characterizations of x%(NiMo₆)@CdS-24 h were investigated by scanning electron microscopy (SEM) and high-resolution transmission electron microscopy (HRTEM) as depicted in Figures 2a–i and 3a–g, respectively. It can be seen in Figure 2 that polyhedral CdS particles exposing terrace facets on the corners were decorated with stacked thin slices. Comparing Figure 2a,d,g, the average crystal size of CdS, which was estimated from SEM images, exhibited a decreasing trend with the increasing hydrothermal time. In Figures 3 and 4a,b, a detailed understanding of crystal structure and morphology was provided by HRTEM measurements equipped with bright field (BF) and high-angle annular dark-field (HAADF) modes. As illustrated in Figure 3a–c, bulk polyhedral CdS particles were loaded with stacked structures that were speculated as NiO/MoS₂ layers according to Reference [10]. Furthermore, in Figure 3d,e, two specified areas highlighted by the square were targeted at the stacked layers (Figure 3g) and the interfacial region (Figure 3f), respectively. More specifically, the lattice distances in these two regions were measured. In the interfacial region (red square box 1),

two lattice fringes with the space of 0.210 and 0.317 nm, corresponding to the (200) plane of NiO (Jade card No.47-1049) and (101) plane of CdS (Jade card No. 65-3414) respectively, were observed in Figure 3f. The amplified HRTEM image of the stacked structure (yellow square box 2) in Figure 3g showed the coexistence of 0.210 and 0.940 nm spacing lattice fringes [25], which were referred to as NiO and 1T-MoS₂, respectively. Through the identification of lattice constant in amplified HRTEM images, a preliminary conclusion that the composite of 1T-MoS₂ doping with NiO was decorated as the layer structure on bulk CdS particle has been raised so far. Moreover, the chemical composition and element distribution of stacked structures were further determined by element mapping. It is worth noting in Figure 4 that the stacked structures marked in a circle were mainly composed of Mo and S elements, whereas no Cd element was found. Besides, the Ni element was also observed in the red circle and bulk particle simultaneously, which can be considered that Ni atoms dope in MoS₂ and bulk CdS particle with a uniform distribution. The HRTEM mapping results also supported the speculation of NiO/1T-MoS₂ structure.

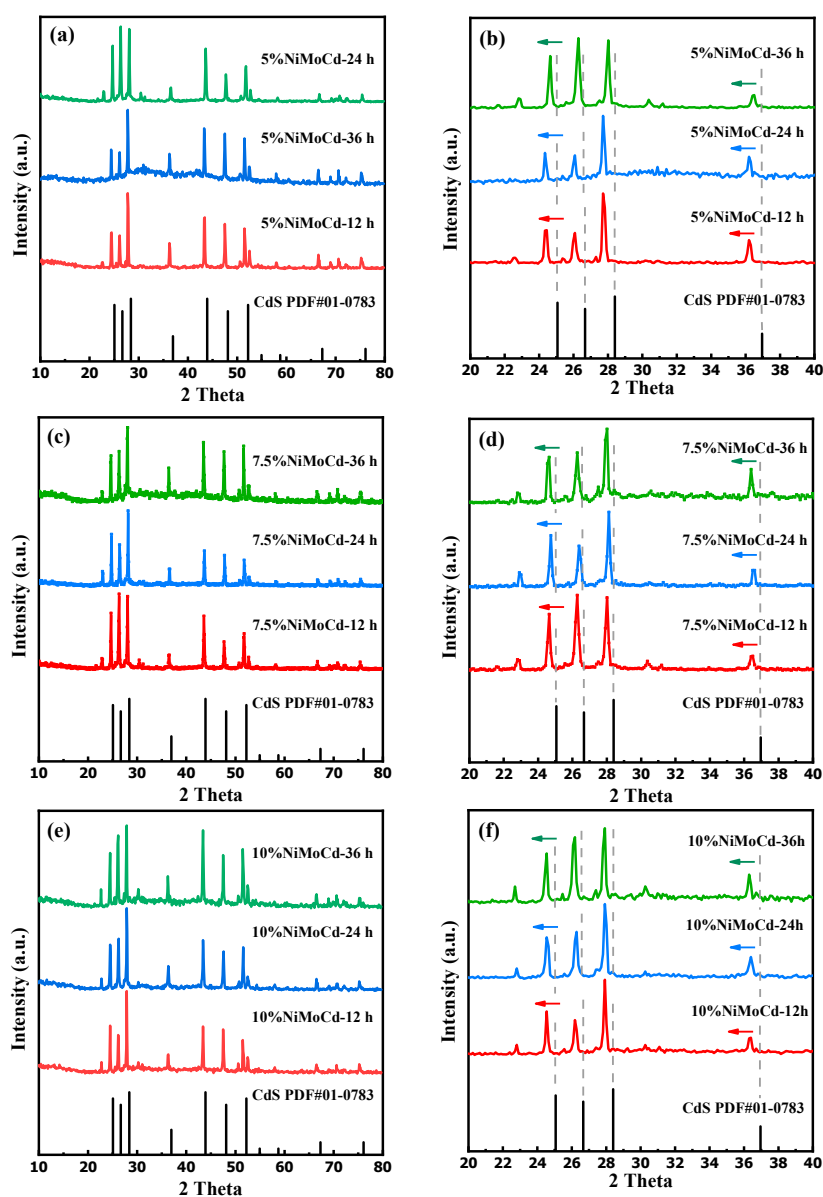


Figure 1. (a–f) XRD patterns of CdS modified with $x\%$ NiMo₆ precursor after different hydrothermal time, τ . Full patterns ranging from 10° to 80° : (a) $x = 5$, (c) $x = 7.5$ and (e) $x = 10$, and amplified patterns ranging from 20° to 40° : (b) $x = 5$, (d) $x = 7.5$ and (f) $x = 10$.

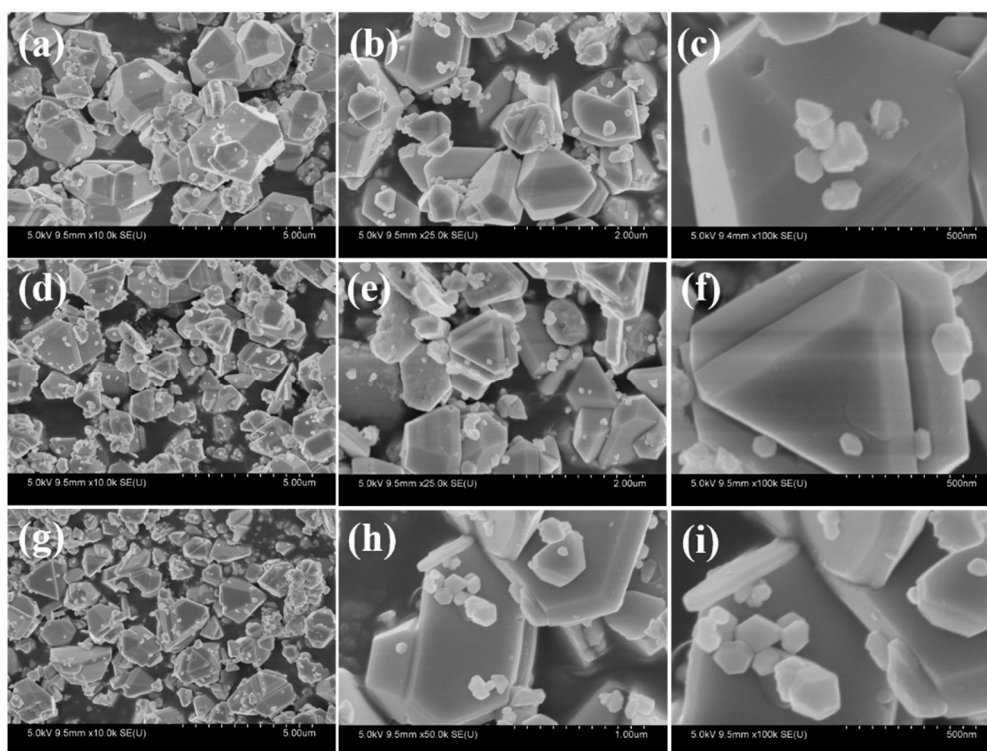


Figure 2. SEM images of (a–c) 5%, (d–f) 7.5% and (g–i) 10% (NiMo₆)@CdS-24 h composites.

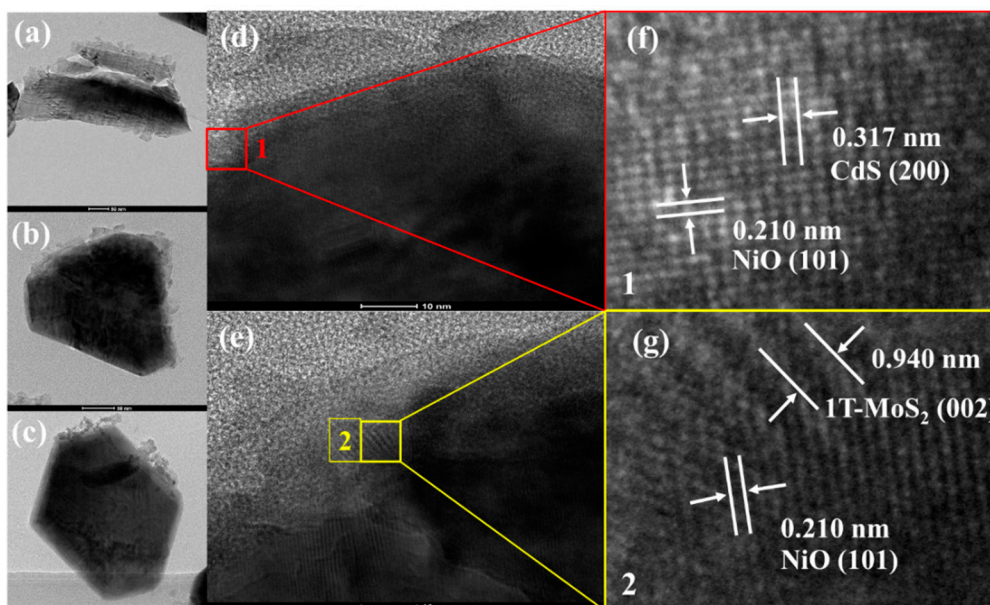


Figure 3. HRTEM images of 5%(NiMo₆)@CdS-24 h composite. (a–c) HRTEM images with a scale bar of 50 nm. (d,e) HRTEM images with a scale bar of 10 nm. (f,g) Amplified specific regions in (f) red square box 1 and (g) yellow square box 2 derived from (d,e), respectively.

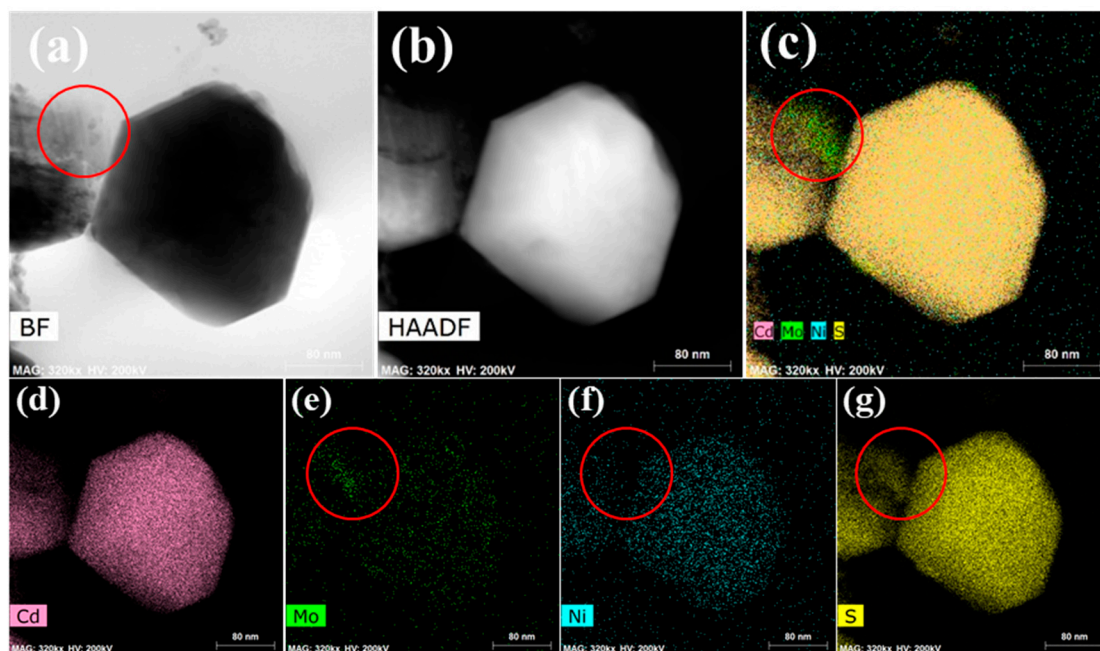


Figure 4. (a) BF image, (b) HAADF image and element mapping of (d) Cd, (e) Mo, (f) Ni, (g) S and (c) overall maps of 5%(NiMo₆)@CdS-24 h composite.

For the purpose of unveiling the definite crystalline structure of NiMo-containing stacks on the CdS surface, the 5%(NiMo₆)@CdS-24 h sample was probed by X-ray photoelectron spectrum (XPS) measurements. As indicated in Figure 5a, two characteristic signals referred to as Cd²⁺ 3d_{5/2} and Cd²⁺ 3d_{3/2}, of which binding energy was located at 404.8 and 411.5 eV respectively, both exhibited a 0.2 eV blueshift in comparison with pure CdS [9,18,26]. The S 2p spectrum in Figure 5b was deconvoluted into three characteristic peaks appearing at 161.2, 162.5 and 164.5 eV, which can be assigned to S²⁻ 2p_{3/2}, S²⁻ 2p_{1/2} [9,18,27] and S₂²⁻ [28], respectively. Similarly, compared with pure CdS, these peaks in the S 2p spectrum showed a slight blueshift ranging from 0.1 to 0.4 eV. The blue shift of Cd 3d and S 2p spectrum resulted from the decoration of NiMo-containing composite that slightly changed the chemical state of bulk CdS.

The Mo 3d spectrum in Figure 5c was characterized by three main peaks referred to as Mo⁴⁺ 3d_{5/2}, Mo⁴⁺ 3d_{3/2} and Mo⁶⁺, implying the existence of Mo⁴⁺ species in (NiMo₆)@CdS. Furthermore, the peaks of Mo⁴⁺ 3d_{5/2} and Mo⁴⁺ 3d_{3/2} appeared at 229.0 and 232.3 eV respectively, which were in accordance with bare 1T-MoS₂ published in previous reports [9,18] and no additional Mo⁴⁺ signal was observed. That said, it is 1T-MoS₂ rather than 2H-MoS₂ or other Mo-containing compounds that were modified on bulk CdS particles, exactly falling in line with the anticipation through this template-based synthetic strategy.

On the contrary, according to our group's previous work [11], 1T and 2H phases of MoS₂ can coexist as the mixed-phase in MoS₂@CdS composites. It seems to inevitably generate a mixed phase of MoS₂ while modifying CdS photocatalyst [9,26]. By contrast, the above observation of pure 1T-MoS₂ phase could be ascribed to the dopant Ni, which might facilitate the transformation from the coexistence of 1T- and 2H-MoS₂ to a mere 1T-MoS₂ phase. According to the previous study, NiMo₆ precursor was introduced as the template to fabricate the NiO/1T-MoS₂ composite structure that was decorated on CdS particles, where 1T-MoS₂ was stabilized by NiO species [10]. Meanwhile, due to the n-type doping, Mo atoms donate electrons to Ni atoms (n-type dopants) and act as the positive charge centers, resulting in the upshift in Mo 3d spectrum, as same to the similar upshift in Cd 3d spectrum. Besides, the appearance of Mo⁶⁺ species can be attributed to partial oxidation of Mo⁴⁺ in the synthesis procedure [10,18,29]. The above findings indicate an intriguing possibility that

NiO/1T-MoS₂@CdS photocatalysts were successfully prepared by the introduction of NiMo₆ precursors into the CdS photocatalyst.

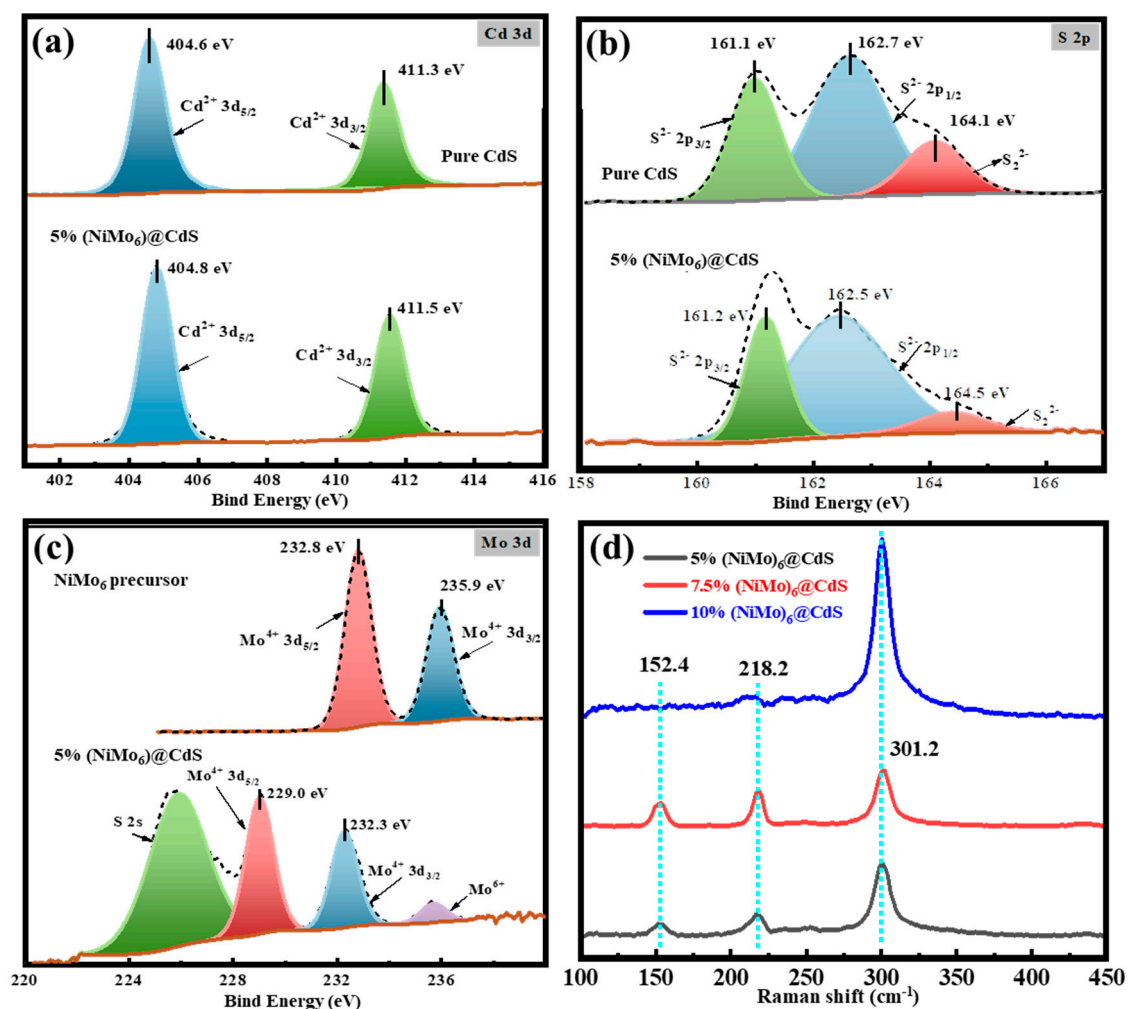


Figure 5. X-ray photoelectron spectrum of 5%(NiMo₆)@CdS-24 h composite, (a) Cd spectrum, (b) S spectrum, (c) Mo spectrum. (d) Raman spectra of x%(NiMo₆)@CdS-24 h composites.

Raman spectra were conducted to obtain further insight into the phase of MoS₂ on the surface of CdS. As illustrated in Figure 5d, two intensive peaks of the Raman shift which appeared at 152.4 and 218.2 cm⁻¹ [30] were detected, respectively. It further substantiates the existence of the 1T-MoS₂ phase, whereas no observation of the 2H-MoS₂ phase was found. It keeps in agreement with the XPS analysis discussed above. Surprisingly no obvious peak referred to 1T-MoS₂ was observed in 10%(NiMo₆)@CdS sample, which inferred that 1T-MoS₂ was almost covered by excess NiO once the amount of NiMo₆ precursor increased over 10%.

As the first step of the three main steps in photocatalysis, the optical absorption of photocatalysts is of necessity to enhance photocatalytic performance [31], which can be reflected by UV-vis diffuse reflection spectrum (UV-vis DRS). As illustrated in Figure 6a, pure CdS and 10%(NiMo₆)@CdS-24 h samples had an approximate band edge position at nearly 515 and 555 nm, respectively. The absorption band edge positions of 5% and 7.5%(NiMo₆)@CdS-24 h samples were at around 540 nm. According to the Tauc plot method, the band gap of semiconductor catalysts was calculated. As presented in Figure 6b, the 10%(NiMo₆)@CdS-24 h sample had a band gap at around 2.24 eV, which was narrower than 5% (2.32 eV), 7.5%(NiMo₆)@CdS-24 h samples (2.28 eV) and pure CdS (2.40 eV). Moreover, the light absorption ability of 5%(NiMo₆)@CdS-24 h composite was superior to the pristine CdS photocatalyst and NiMo₆ precursor in Figure 6c,d. Therefore, the modification with NiO/1T-MoS₂ on bulk CdS

photocatalyst broadened the absorption of the light wavelength range [27,32]. The enhancement of absorption ability can be attributed to the heterojunction among NiO, 1T-MoS₂ and CdS [32,33]. Additionally, the tailing region of light absorption was intensified, which could be ascribed to the increasing amount of MoS₂ with a broad absorption range in visible light [34,35].

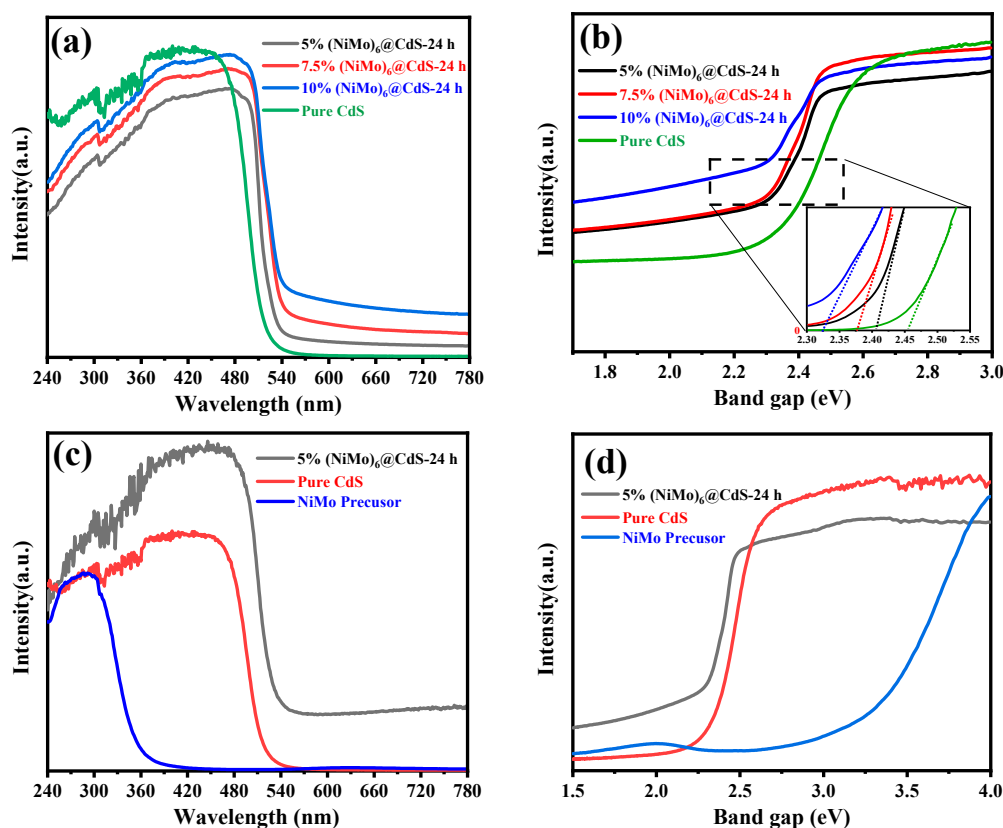


Figure 6. (a,c) UV-vis DRS and (b,d) band gap of $x\%(\text{NiMo}_6)\text{@CdS-24 h}$ composites compared with pure CdS and NiMo₆ precursor.

Accumulated hydrogen evolution of $x\%(\text{NiMo}_6)\text{@CdS-}\tau$ samples was recorded as illustrated in Figure 7a–f. Typically, loading noble metal Pt as a co-catalyst on CdS photocatalyst enhances the photocatalytic performance. As shown in Figure 7e, (NiMo₆)@CdS samples with non-noble metal all displayed a remarkable improvement in photocatalytic activity, which was comparable or even superior to the optimal Pt-CdS in the literature [36]. With regard to the hydrothermal time, τ , in Figure 7b–d, the (NiMo₆)@CdS-24 h sample was endowed with the best photocatalytic performance. It infers that the (NiMo₆)@CdS-24 h sample was prepared in suitable particle size and modified with a uniform distribution of NiO/1T-MoS₂ after moderate hydrothermal time of 24 h, which accounts for its outstanding activity compared with the other hydrothermal times. Furthermore, as we can see in Figure 7a, the 5%(NiMo₆)@CdS sample exhibited the highest photocatalytic activity with a hydrogen evolution rate of 348.5 $\mu\text{mol/h}$, whereas 7.5% and 10%(NiMo₆)@CdS samples showed a relatively lower rate of 301.1 and 253.7 $\mu\text{mol/h}$, under the same hydrothermal time of 24 h. This difference of photocatalytic performance between variable precursor amounts can be explained by the influence of the modification with the special layer structure of NiO/1T-MoS₂, which is clarified as mentioned below. Additionally, combined with the analysis of optical absorption, Figure 7f showed that the 5%(NiMo₆)@CdS sample performed an excellent photocatalytic activity within the visible light region. Photocatalytic stability was evaluated by intermittent test sequences and each sequence consisted of the consecutive hydrogen measurement for 5 h. After one test sequence, the photocatalysts were reused through suction filtration and drying in a vacuum. Then, the photocatalytic reactor with photocatalysts inside was evacuated again and then irradiated for the next round. As illustrated

in Figure 8a, the 5%(NiMo)₆@CdS-24 h composite maintained a relatively stable photocatalytic performance through three cycles. In the last stability test cycle, the average hydrogen evolution per hour had decreased to approximately 90% compared to the initial cycle. In Figure 8b, the XRD pattern of the after-test sample was conducted in comparison with the before-test one. As illustrated in Figure 8b, there was no obvious difference in the characteristic peaks, which indicated that the photo-corrosion phenomenon was not observed from the XRD result and the main structure of CdS was maintained. Therefore, the photocatalytic performance reduction can be attributed to the mass loss of photocatalysts in the suction filtration and drying process. As mentioned above, the introduction of NiO species could stabilize the 1T-MoS₂ structure, which could probably result in the stable photocatalytic activity of NiMo-CdS samples. However, the intrinsic stabilization mechanism of NiMo-CdS photocatalysts needs to be further explored in future research.

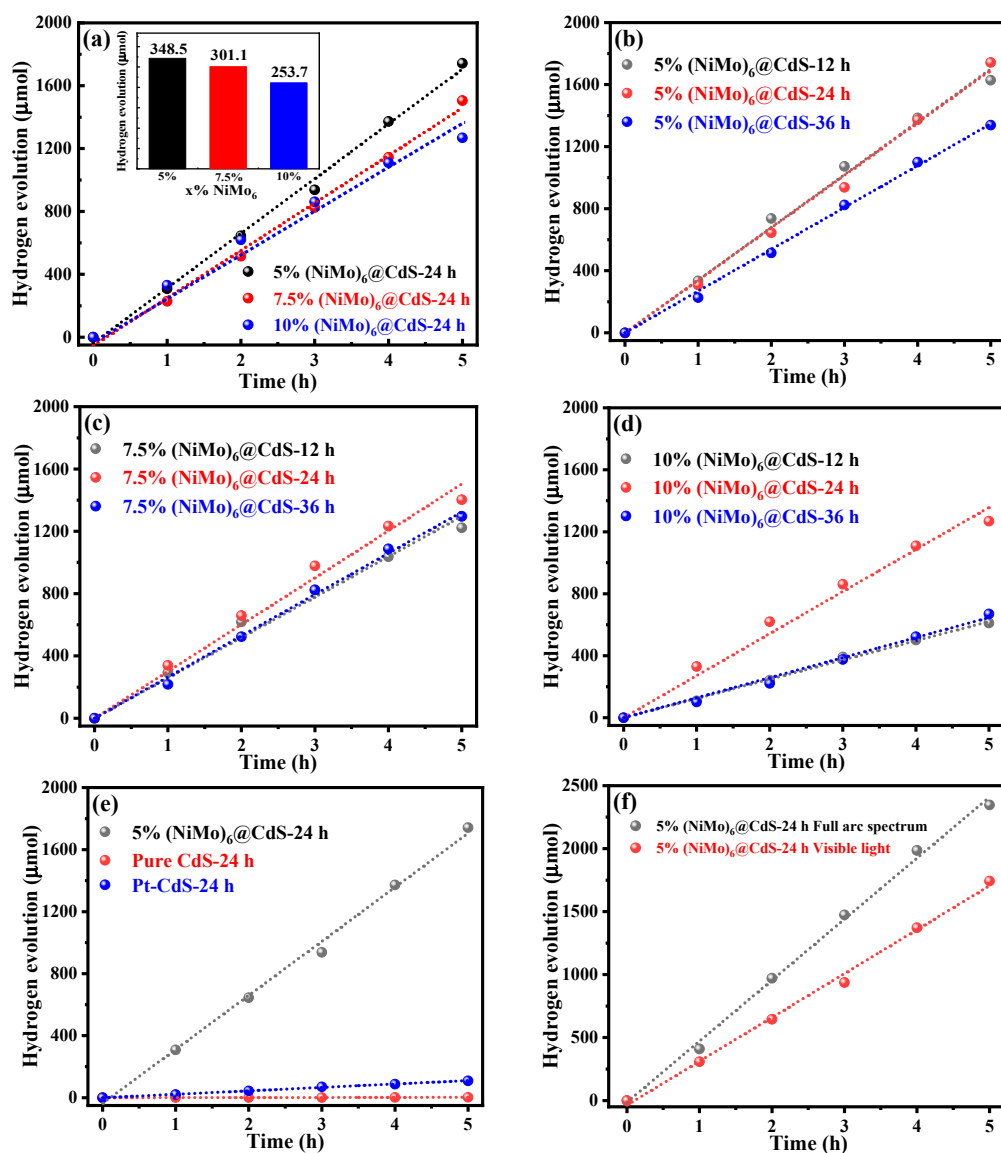


Figure 7. (a–f) Photocatalytic hydrogen evolution performance: 50 mg catalysts dispersed in 100 mL aqueous solution containing 20 vol% of 0.05/0.07 mol/L Na₂S/Na₂SO₃. (a) Variable x% amounts of NiMo₆, (b–d) with variable hydrothermal time of 12, 24 and 36 h in series of (b) 5%, (c) 7.5% and (d) 10%(NiMo)₆@CdS composites. (f) Comparison between full arc spectrum and visible spectrum. All the hydrogen evolution measurements were conducted under irradiation within the visible spectrum, except for (f).

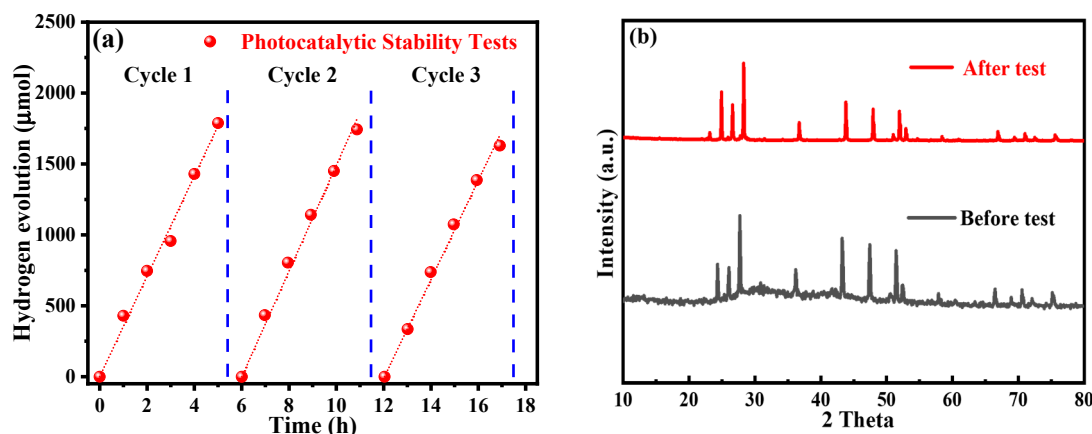


Figure 8. (a) Photocatalytic stability tests and (b) XRD patterns of the 5%(NiMo₆)@CdS-24 h composite before and after photocatalytic measurements.

The influence mechanism of the modification with NiO/1T-MoS₂ on pristine CdS photocatalyst can be elucidated from two primary perspectives. Through the polyoxometalate template-based synthetic strategy with NiMo₆ precursor [10], NiO/1T-MoS₂ was successfully loaded on the bulk CdS surface and stacked together to eventually form the thick layer structures. On the one hand, due to the superior absorption ability of 1T-MoS₂ [33–35], the thicker layer structure containing more NiO/1T-MoS₂ can absorb a larger proportion of the incident light, which in turn suppresses the excitation of photo-induced electron and hole pairs inside CdS photocatalysts and further diminishes the total photocatalytic efficiency of the NiO/1T-MoS₂@CdS composite. In other words, the excessive coverage of NiO/1T-MoS₂ restrains the optical absorption of bulk CdS photocatalyst and hence the total photocatalytic performance is bound to reduce to some extent. On the other side, the effective photocatalysis reacts in the prerequisite that the photo-excited carriers separated inside the bulk CdS particle successfully transfer to the surface of Ni/1T-MoS₂ layer structures, where the interfacial chemical reaction occurs. It is reasonable to speculate that the 1T-MoS₂ layer structure as its excellent conductivity [37,38] enhances the transportation of electrons through its suitable layer structure and simultaneously inhibits the combination of photo-excited charges in CdS particles. NiO species, distributed uniformly on the surface of both CdS particles and 1T-MoS₂ layers, exhibit high activity in proton reduction [22,24]. Therefore, NiO and 1T-MoS₂ loaded as bi-metal co-catalysts both play a vital role in promoting proton reduction, ultimately accelerating the hydrogen evolution. Having said that, the substantial interaction between NiO/1T-MoS₂ with bulk CdS need to be further investigated with in-depth studies, and the migration mechanism of photo-induced electrons inside NiO/1T-MoS₂ layers have not yet been fully clarified.

3. Experimental Methods and Characterizations

3.1. Materials

All chemicals were obtained as analytic reagent chemicals unless otherwise noted. Ammonium molybdate tetrahydrate ((NH₄)₆Mo₇O₂₄·4H₂O), nickel nitrate hexahydrate (Ni(NO₃)₂·6H₂O) and cadmium nitrate tetrahydrate (Cd(NO₃)₂·4H₂O) were bought from Beijing InnoChem technology Co., Ltd. (Beijing, China). Thioacetamide (CH₃CSNH₂) was purchased from Sinopharm Chemical Reagent Co., Ltd. (Beijing, China). Ultra-pure water with a resistivity of 18.2 MΩ·cm was used throughout all of the experiments.

3.2. Synthesis of NiMo₆ Precursor (NH₄)₄[NiH₆Mo₆O₂₄]·5H₂O

The NiMo₆ precursor (NH₄)₄[NiH₆Mo₆O₂₄]·5H₂O was prepared based on the modified experimental procedure in the previous report [10]. 4.2 mmol of (NH₄)₆Mo₇O₂₄·4H₂O was dissolved in

80 mL ultra-pure water and the solution was heated to 80 °C and then stirred for 1 h, which was referred to as Mo-Solution. 4 mmol of $\text{Ni}(\text{NO}_3)_2 \cdot 6\text{H}_2\text{O}$ was dissolved in 20 mL ultra-pure water, which was referred to as Ni-Solution. Next, the latter Ni-Solution was added dropwise to the former Mo-Solution and was stirred for 5 h at 80 °C. Subsequently, 80 mL ultra-pure water was added, after which the solution was heated to 100 °C and stirred for 1 h. Finally, after the solution was naturally cooled down to room temperature, the obtained NiMo_6 products were washed several times by centrifugation with distilled water and dried at 80 °C for 12 h under vacuum.

3.3. Synthesis of $x\%(\text{NiMo}_6)@\text{CdS}$ - τ ($\tau = 12, 24, 36$ h)

$(\text{NiMo}_6)@\text{CdS}$ particles with variable amounts of NiMo_6 were fabricated by a conventional hydrothermal reaction method. 36 mmol of CH_3CSNH_2 was dissolved into 50 mL ultra-pure water and the solution was sonicated for 5 min. After sonication, the solution was stirred for 1 h. Then, 5 mmol of $\text{Cd}(\text{NO}_3)_2 \cdot 4\text{H}_2\text{O}$ and variable amounts of NiMo_6 precursor ($x\% \times 5$ mmol NiMo_6) were introduced into the CH_3CSNH_2 aqueous solution, respectively. After continuous magnetic stirring for 6 h, the thorough stirring solution was transferred into a 100 mL Teflon-lined stainless-steel autoclave and heated at 200 °C for periods ranging from 12 to 36 h. After being washed 5–6 times by centrifugation with distilled water and dried at 80 °C for 12 h under vacuum, the brownish-yellow $x\%(\text{NiMo}_6)@\text{CdS}$ - τ products were obtained, where x and τ represent the mole fraction of NiMo_6 precursor and hydrothermal time, respectively.

3.4. Synthesis of Pt-CdS

Pt-CdS photocatalyst was prepared by the photo-deposition method. Typically, with H_2PtCl_6 as a precursor, the co-catalyst Pt with a mass ratio of 0.2% compared to the samples, was loaded on pure CdS photocatalyst via the photo-deposition method, in the presence of 80 mL of methanol solution (25 vol%). After the suction filtration, all solid samples were dried at 80 °C for 12 h in a vacuum and then the Pt-CdS photocatalyst was collected and obtained as the experimental control group.

3.5. Characterizations

To identify the crystalline phase and the composition of the obtained photocatalysts, powder X-ray diffraction patterns were measured on an X-ray diffractometer (D8 Advance, Bruker, Karlsruhe, Germany) equipped with $\text{Cu-K}\alpha$ as the X-ray source at 40 kV voltage and 15 mA current. The diffraction angle (2θ) range was from 10° to 80° with a scan speed of 5°/min. The powder X-ray diffraction patterns were further analyzed by Jade 6.0 software. The surface morphology of obtained photocatalysts was unveiled by scanning electron microscopy (SEM) (JSM-6700, JEOL, Tokyo, Japan) and high-resolution field-emission transmission electron microscopy (HRTEM) with element mapping (TALOS F200X, FEI, Hillsborough, OR, USA). The chemical composition and electronic state of obtained photocatalysts were derived from X-ray photoelectron spectroscopy (XPS) conducted by an X-ray photoelectron spectrometer (AXIS UltraDLD, Kratos, Manchester, UK) with $\text{Mg-K}\alpha$ radiation. Raman spectra measurement was performed on a dispersive Raman microscope (Senterra R200-L, Bruker Optics, Karlsruhe, Germany) with the excitation wavelength of 520 nm. The optical absorption property of obtained photocatalysts was reflected by UV-vis diffuse reflection spectra (DRS) on a UV-Vis spectrophotometer (UV-2450, Shimadzu, Kyoto, Japan) with BaSO_4 as the reference.

3.6. Photocatalytic Activity Measurements

The particulate photocatalytic hydrogen evolution was conducted in a 300 mL Pyrex glass reactor under irradiation under visible light, using a 300 W Xe-lamp (CEL-HXF300, Beijing China Education Au-light Co., Ltd., Beijing, China) equipped with an optical filter ranging from 420 to 780 nm, followed with a closed gas circuit system connected with a vacuum pump and online gas chromatography (Huaai GC9160, Huaai, Shanghai, China). 50 mg of $(\text{NiMo}_6)@\text{CdS}$ sample was dispersed in an aqueous solution (100 mL) containing 20 vol% 0.05/0.07 mol/L $\text{Na}_2\text{S}/\text{Na}_2\text{SO}_3$ through the 10 min sonication.

The photocatalytic reactor was pumped to vacuum to evacuate the dissolved air in the solution. The photocatalysts were in suspension with continuous magnetic stirring while being exposed to light irradiation. The amount of hydrogen evolved per hour was determined by the online gas chromatography equipped with argon as a carrier gas.

4. Conclusions

In summary, a series of Ni, Mo co-doped CdS photocatalysts with non-noble metal such as Pt, have been prepared by polyoxometalate template-based synthetic strategy with NiMo₆ precursor. 1T-MoS₂ stabilized by the introduction of NiO together with stacking layer structures was successfully decorated on the terrace facets of bulk CdS particles. Due to the modification of the special layer structure, NiO/1T-MoS₂@CdS composites exhibited a greater photocatalytic performance than pristine Pt-loaded CdS, among which the 5%(NiMo₆)@CdS sample stood out for its best hydrogen evolution activity with approximately 348.5 μmol/h, in the presence of Na₂S/Na₂SO₃. The AQY efficiency could reach to 42% at 365 nm. The above results illustrated that NiO and 1T-MoS₂ have a synergistic effect on enhancing the separation efficiency of photoexcited electron and hole pairs in CdS and facilitating the interfacial proton reduction, namely hydrogen evolution, at the surface-active site. However, the more detailed charge transfer procedure through the NiO/1T-MoS₂ layer structure still needs clarifying in future research.

Author Contributions: J.Y.—Validation, Writing—original draft, Conceptualization, Visualization, Investigation and Data curation; Z.W.—Formal analysis; M.X.—Methodology; Z.J.—Supervision; W.S.—Writing—review and editing, Project administration and Funding acquisition. All authors have read and agreed to the published version of the manuscript.

Funding: This research was supported by the National Key Basic Research and Development Program (2018YFB1502001), the National Natural Science Foundation of China (21773153), Centre of Hydrogen Science, Shanghai Jiao Tong University, China.

Acknowledgments: We show our gratitude to the engineers and technicians in Instrumental Analysis Center, Shanghai Jiao Tong University, China.

Conflicts of Interest: The authors declared that they have no conflict of interest.

References

1. Fujishima, A.; Honda, K. Electrochemical photolysis of water at a semiconductor electrode. *Nature* **1972**, *238*, 37–38. [[CrossRef](#)]
2. Hitoki, G.; Takata, T.; Kondo, J.N.; Hara, M.; Kobayashi, H.; Domen, K. An oxynitride, TaON, as an efficient water oxidation photocatalyst under visible light irradiation ($\lambda \leq 500$ nm). *Chem. Commun.* **2002**, *16*, 1698–1699. [[CrossRef](#)]
3. Wang, X.C.; Maeda, K.; Thomas, A.; Takanabe, K.; Xin, G.; Carlsson, J.M.; Domen, K.; Antonietti, M. A metal-free polymeric photocatalyst for hydrogen production from water under visible light. *Nat. Mater.* **2008**, *8*, 76–80. [[CrossRef](#)]
4. Wagner, F.T.; Somorjai, G.A. Photocatalytic and photoelectrochemical hydrogen production on strontium titanate single crystals. *J. Am. Chem. Soc.* **1980**, *102*, 5494–5502. [[CrossRef](#)]
5. Tokunaga, S.; Kato, H.; Kudo, A. Selective Preparation of monoclinic and tetragonal BiVO₄ with scheelite structure and their photocatalytic properties. *Chem. Mater.* **2001**, *13*, 4624–4628. [[CrossRef](#)]
6. Yuan, J.; Chen, M.X.; Shi, J.W.; Shangguan, W.F. Preparations and photocatalytic hydrogen evolution of N-doped TiO₂ from urea and titanium tetrachloride. *Int. J. Hydrogen Energy* **2006**, *31*, 1326–1331. [[CrossRef](#)]
7. Schneider, J.; Matsuoka, M.; Takeuchi, M.; Zhang, J.; Horiuchi, Y.; Anpo, M.; Bahnemann, D.W. Understanding TiO₂ photocatalysis: Mechanisms and materials. *Chem. Rev.* **2014**, *114*, 9919–9986. [[CrossRef](#)]
8. Hashimoto, K.; Irie, H.; Fujishima, A. TiO₂ photocatalysis: A historical overview and future prospects. *Jpn. J. Appl. Phys.* **2005**, *44*, 8269–8285. [[CrossRef](#)]
9. Xu, M.Q.; Wei, Z.D.; Liu, J.Y.; Guo, W.Q.; Zhu, Y.; Chi, J.S.; Jiang, Z.; Shangguan, W.F. One-pot synthesized visible-light-responsive MoS₂@CdS nanosheets-on- nanospheres for hydrogen evolution from the antibiotic wastewater: Waste to energy insight. *Int. J. Hydrogen Energy* **2019**, *44*, 21577–21587. [[CrossRef](#)]

10. Wei, Z.D.; Xu, M.Q.; Liu, J.Y.; Guo, W.Q.; Jiang, Z.; Shangguan, W.F. Simultaneous visible-light-induced hydrogen production enhancement and antibiotic wastewater degradation using MoS₂@ZnxCd_{1-x}S: Solid-solution-assisted photocatalysis. *Chin. J. Catal.* **2020**, *41*, 103–113. [\[CrossRef\]](#)
11. Kumar, D.P.; Hong, S.; Reddy, D.A.; Kim, T.K. Noble metal-free ultrathin MoS₂ nanosheet-decorated CdS nanorods as an efficient photocatalyst for spectacular hydrogen evolution under solar light irradiation. *J. Mater. Chem. A* **2016**, *4*, 18551–18558. [\[CrossRef\]](#)
12. Huang, Y.C.; Sun, Y.H.; Zheng, X.L.; Aoki, T.; Pattengale, B.; Huang, J.E.; He, X.; Bian, W.; Younan, S.; Williams, N.; et al. Atomically engineering activation sites onto metallic 1T-MoS₂ catalysts for enhanced electrochemical hydrogen evolution. *Nat. Commun.* **2019**, *10*, 982. [\[CrossRef\]](#)
13. Qiu, B.C.; Zhu, Q.H.; Du, M.M.; Fan, L.G.; Xing, M.Y.; Zhang, J.L. Efficient solar light harvesting CdS/Co₉S₈ hollow cubes for Z-scheme photocatalytic water splitting. *Angew. Chem. Int. Ed.* **2017**, *56*, 2684–2688. [\[CrossRef\]](#)
14. Xu, X.J.; Hu, L.F.; Gao, N.; Liu, S.X.; Wageh, S.; Al-Ghamdi, A.A.; Alshahrie, A.; Fang, X.S. Controlled growth from ZnS nanoparticles to ZnS-CdS nanoparticle hybrids with enhanced photoactivity. *Adv. Funct. Mater.* **2015**, *25*, 445–454. [\[CrossRef\]](#)
15. Fang, X.Y.; Cui, L.F.; Pu, T.T.; Song, J.L.; Zhang, X.D. Core-shell CdS@MnS nanorods as highly efficient photocatalysts for visible light driven hydrogen evolution. *Appl. Surf. Sci.* **2018**, *457*, 863–869. [\[CrossRef\]](#)
16. Zhang, J.; Wang, Y.H.; Jin, J.; Zhang, J.; Lin, Z.; Huang, F.; Yu, J.G. Efficient visible-light photocatalytic hydrogen evolution and enhanced photostability of core/shell CdS/g-C₃N₄ nanowires. *ACS Appl. Mater. Interfaces* **2013**, *5*, 10317–10324. [\[CrossRef\]](#)
17. Wu, X.Q.; Zhao, J.; Wang, L.P.; Han, M.M.; Zhang, M.L.; Wang, H.B.; Huang, H.; Liu, Y.; Kang, Z.H. Carbon dots as solid-state electron mediator for BiVO₄/CDs/CdS Z-scheme photocatalyst working under visible light. *Appl. Catal. B Environ.* **2017**, *206*, 501–509. [\[CrossRef\]](#)
18. Chang, K.; Hai, X.; Pang, H.; Zhang, H.B.; Shi, L.; Liu, G.G.; Liu, H.M.; Zhao, G.X.; Li, M.; Ye, J.H. Targeted synthesis of 2H- and 1T-phase MoS₂ monolayers for catalytic hydrogen evolution. *Adv. Mater.* **2016**, *28*, 10033–10041. [\[CrossRef\]](#)
19. Zhang, X.H.; Li, N.; Wu, J.; Zheng, Y.Z.; Tao, X. Defect-rich O-incorporated 1T-MoS₂ nanosheets for remarkably enhanced visible-light photocatalytic H₂ evolution over CdS: The impact of enriched defects. *Appl. Catal. B Environ.* **2018**, *229*, 227–236. [\[CrossRef\]](#)
20. Liu, Q.; Shang, Q.C.; Khalil, A.; Fang, Q.; Chen, S.M.; He, Q.; Xiang, T.; Liu, D.B.; Zhang, Q.; Luo, Y.; et al. In situ integration of a metallic 1T-MoS₂/CdS heterostructure as a means to promote visible-light-driven photocatalytic hydrogen evolution. *ChemCatChem* **2016**, *8*, 2614–2619. [\[CrossRef\]](#)
21. Lian, Z.Q.; Liu, Y.C.; Liu, H.; Zhou, H.L.; Chang, Z.D.; Li, W.J. Fabrication of CdS@1T-MoS₂ core-shell nanostructure for enhanced visible-light-driven photocatalytic H₂ evolution from water splitting. *J. Taiwan Inst. Chem. E* **2019**, *105*, 57–64. [\[CrossRef\]](#)
22. Qiao, S.S.; Feng, C.; Guo, Y.; Chen, T.X.; Akram, N.; Zhang, Y.; Wang, W.; Yue, F.; Wang, J.D. CdS nanoparticles modified Ni@NiO spheres as photocatalyst for oxygen production in water oxidation system and hydrogen production in water reduction system. *Chem. Eng. J.* **2020**, *395*, 125068. [\[CrossRef\]](#)
23. Khan, Z.; Khannam, M.; Vinothkumar, N.; De, M.; Qureshi, M. Hierarchical 3D NiO–CdS heteroarchitecture for efficient visible light photocatalytic hydrogen generation. *J. Mater. Chem.* **2012**, *22*, 12090. [\[CrossRef\]](#)
24. Chen, X.P.; Chen, W.; Gao, H.Y.; Yang, Y.; Shangguan, W.F. In situ photodeposition of NiO_x on CdS for hydrogen production under visible light: Enhanced activity by controlling solution environment. *Appl. Catal. B Environ.* **2014**, *152–153*, 68–72. [\[CrossRef\]](#)
25. Li, Z.Y.; Fan, R.Y.; Hu, Z.; Li, W.C.; Zhou, H.J.; Kang, S.D.; Zhang, Y.X.; Zhang, H.M.; Wang, G.Z. Ethanol introduced synthesis of ultrastable 1T-MoS₂ for removal of Cr(VI). *J. Hazard. Mater.* **2020**, *394*, 122525. [\[CrossRef\]](#)
26. Yin, X.L.; Li, L.L.; Jiang, W.J.; Zhang, Y.; Zhang, X.; Wan, L.J.; Hu, J.S. MoS₂/CdS nanosheets-on-nanorod heterostructure for highly efficient photocatalytic H₂ generation under visible light irradiation. *ACS Appl. Mater. Interfaces* **2016**, *8*, 15258–15266. [\[CrossRef\]](#)
27. Han, B.; Liu, S.; Zhang, N.; Xu, Y.J.; Tang, Z.R. One-dimensional CdS@MoS₂ core-shell nanowires for boosted photocatalytic hydrogen evolution under visible light. *Appl. Catal. B Environ.* **2017**, *202*, 298–304. [\[CrossRef\]](#)
28. Colvin, V.L.; Goldstein, A.N.; Alivisatos, A.P. Semiconductor nanocrystals covalently bound to metal surfaces with self-assembled monolayers. *J. Am. Chem. Soc.* **1992**, *114*, 5221–5230. [\[CrossRef\]](#)

29. Wang, L.L.; Liu, X.; Luo, J.M.; Duan, X.D.; Crittenden, J.; Liu, C.B.; Zhang, S.Q.; Pei, Y.; Zeng, Y.X.; Duan, X.F. Self-Optimization of the active site of molybdenum disulfide by an irreversible phase transition during photocatalytic hydrogen evolution. *Angew. Chem. Int. Ed.* **2017**, *56*, 7610–7614. [[CrossRef](#)]
30. Yang, D.; Sandoval, S.J.; Divigalpitiya, W.M.; Irwin, J.C.; Frindt, R.F. Structure of single-molecular-layer MoS₂. *Phys. Rev. B* **1991**, *43*, 12053. [[CrossRef](#)]
31. Chen, S.S.; Takata, T.; Domen, K. Particulate photocatalysts for overall water splitting. *Nat. Rev. Mater.* **2017**, *2*, 1–17. [[CrossRef](#)]
32. Yang, M.Q.; Han, C.; Xu, Y.J. Insight into the effect of highly dispersed MoS₂ versus layer-structured MoS₂ on the photocorrosion and photoactivity of CdS in graphene–CdS–MoS₂ composites. *J. Phys. Chem. C* **2015**, *119*, 27234–27246. [[CrossRef](#)]
33. Lee, H.S.; Min, S.W.; Chang, Y.G.; Park, M.K.; Nam, T.; Kim, H.; Kim, J.H.; Ryu, S.; Im, S. MoS₂ nanosheet phototransistors with thickness-modulated optical energy gap. *Nano Lett.* **2012**, *12*, 3695–3700. [[CrossRef](#)]
34. Li, H.; Lu, G.; Yin, Z.Y.; He, Q.Y.; Li, H.; Zhang, Q.; Zhang, H. Optical identification of single- and few-layer MoS₂ sheets. *Small* **2012**, *8*, 682–686. [[CrossRef](#)]
35. Jia, G.Y.; Liu, Y.; Gong, J.Y.; Lei, D.Y.; Wang, D.L.; Huang, Z.X. Excitonic quantum confinement modified optical conductivity of monolayer and few-layered MoS₂. *J. Mater. Chem. C* **2016**, *4*, 8822–8828. [[CrossRef](#)]
36. Xin, G.; Yu, B.; Xia, Y.J.; Hu, T.; Liu, L.M.; Li, C.F. Highly efficient deposition method of platinum over CdS for H₂ evolution under visible light. *J. Phys. Chem. C* **2014**, *118*, 21928–21934. [[CrossRef](#)]
37. Fivaz, R.; Mooser, E. Mobility of charge carriers in semiconducting layer structures. *Phys. Rev.* **1967**, *163*, 743. [[CrossRef](#)]
38. Souder, A.; Brodie, D.E. Electrical contacts and conductivity of MoS₂ layer structures. *Can. J. Phys.* **1971**, *49*, 2565–2571. [[CrossRef](#)]

Publisher's Note: MDPI stays neutral with regard to jurisdictional claims in published maps and institutional affiliations.



© 2020 by the authors. Licensee MDPI, Basel, Switzerland. This article is an open access article distributed under the terms and conditions of the Creative Commons Attribution (CC BY) license (<http://creativecommons.org/licenses/by/4.0/>).